IEEE Access
Multidisciplinary | Rapid Review | Open Access Journal

Received April 24, 2017, accepted May 21, 2017, date of publication June 23, 2017, date of current version August 8, 2017.

Digital Object Identifier 10.1109/ACCESS.2017.2719048

Voltage Regulation System of Doubly Salient Electromagnetic Generator Based on Indirect Adaptive Fuzzy Control

WEILI DAI[1,2], (Member, IEEE), YANGHUA YU[1,2], MINGANG HUA[1], (Member, IEEE), AND CHANGCHUN CAI [1,2]

[1]College of Internet of Things Engineering, Hohai University, Changzhou 213022, China
[2]Jiangsu Key Laboratory of Power Transmission and Distribution Equipment Technology, Changzhou 213022, China

Corresponding author: Weili Dai (daiwl@hhu.edu.cn)

This work was supported in part by the National Natural Science Foundation of China under Grant 51207043 and Grant 51607057, in part by the Natural Science Foundation of Jiangsu Province under Grant BK2012150, and in part by the Outstanding Innovative Talents Plan of Hohai University.

ABSTRACT In this paper, a voltage regulation system based on indirect adaptive fuzzy (IAF) control for doubly salient electromagnetic generator (DSEG) is proposed to improve the robustness of the system and reduce output voltage ripple. The operating principle of IAF controller is described in detail subsequently and the stability condition of the system is deduced by Lyapunov function based on the mathematical model and working principle of the generator. Moreover, the selection method of parameters and control strategy are determined with the adaptive fuzzy control law. Finally, a field-circuit coupling simulation model of voltage regulation system for DSEG using IAF controller is constructed by finite element analysis technique and transient solver of control circuit. The simulation results show that DSEG using IAF controller has good static characteristics, high robustness, and low output voltage ripple.

INDEX TERMS Doubly salient electromagnetic generator, indirect adaptive fuzzy control, voltage regulation system, field-circuit coupling simulation.

I. INTRODUCTION

Doubly salient permanent magnet machine (DSPM) [1] was proposed by Prof. Lipo in the 1990s, which is similar to switched reluctance machine (SRM) and inherits the merits of simple structure, high efficiency and good robustness. For higher power density compared with SRM, it is widely used in motor drive system [2]. Although DSPM can work as a generator, the flux produced by permanent magnets (PMs) is difficult to be changed. So, output voltage of generator can be regulated only by adding a PWM converter connected with three phase windings of DSPM [3]. To overcome above disadvantages, doubly salient electromagnetic machine (DSEM) [4] and brushless doubly fed doubly salient machine [5] were proposed by replacing PMs with dc field windings. DSEM enhances the reliability in generating mode since there are no power switches in main power circuit and the magnetic field can be eliminated by cutting off the field current as generator operates in faults. Meanwhile, doubly salient hybrid excitation machine (DSHEM) was developed for less field windings and wider speed range [6]. Chen *et al*. [7] discussed flux regulation capability of different DSHEMs when they operate in generating mode. While Le *et al*. [8] analyzed doubly salient generators with different building magnetic field ways and gave a comparison of their output characteristics. The studies show that DSEM and DSHEM are suitable for running as generators for the existence of dc field windings.

The control of voltage regulator is vital for doubly salient generators. Though traditional output voltage feedback plus dc field current feed-forward control [9] can improve dynamic characteristics of generator, the analog control solution is very sensitive to the parameters variation. To improve robustness of the system, the sliding mode (SM) control [10] was applied in voltage regulation system of doubly salient electromagnetic generator (DSEG) and the results verify good robustness and dynamic characteristics. But it still has large overshoot of output voltage. In recent years, the studies about fuzzy control exhibit that it has excellent robustness in nonlinear systems and systems with uncertainties [11], [12]. However, the main drawbacks of

these approaches are lack of stability analysis mechanisms in detailed fields, which limit their applications in engineering practice. So, some researchers combined fuzzy control with other control theories to achieve better performance. Attia *et al.* [13] proposed a genetic algorithm with fuzzy logic controller to realize the adaptive control in the self-excited induction generator. A direct adaptive control schemes with fuzzy logic was proposed in paper [14] and this control method has both merits of adaptive control and fuzzy control. The similar control strategies have been applied in web-based e-service systems [15], MIMO nonlinear systems [16], affine nonlinear systems [17] and strict-feedback nonlinear system [18].

DSEG is a strong electromagnetic coupling and high nonlinear system. For solving large overshoot and keeping good robustness and dynamic performance, a voltage regulation system based on indirect adaptive fuzzy (IAF) control is performed. In this paper, IAF controller with Gaussian-shaped membership functions based on the mathematical model and operating principle of generator is proposed to improve the robustness of DSEG system. Subsequently, the selection solution of control parameters is given by Lyapunov stability method. Finally, a field-circuit coupling simulation model is built, and steady state and dynamic simulation have been done to demonstrate that the voltage regulation system of DSEG based on IAF control has lower voltage ripple and stronger load characteristics compared with Fuzzy PID control.

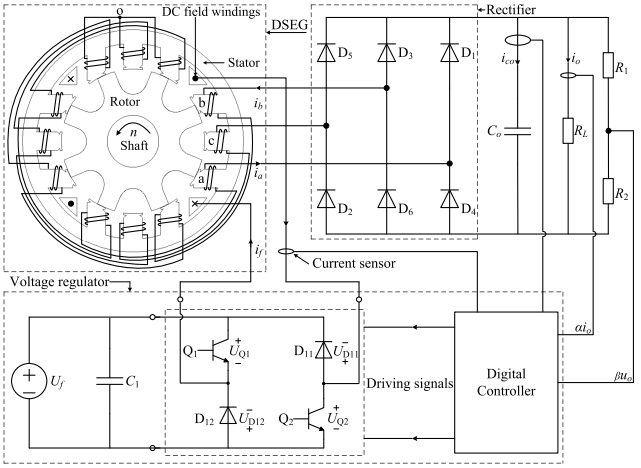

FIGURE 1. The scheme of DSEG system.

II. VOLTAGE REGULATION SYSTEM OF DSEG

As shown in Fig. 1, DSEG system is usually composed of three components: DSEG, voltage regulator and three-phase rectifier. Three phase windings are connected with three-phase rectifier so that alternative current source outputted by the generator can be turned into direct current source.

A. STRUCTURE AND MATHEMATICAL MODEL OF DSEG

Structure and finite element analysis model of 12/8 poles DSEG are shown in Fig. 2 and corresponding parameters

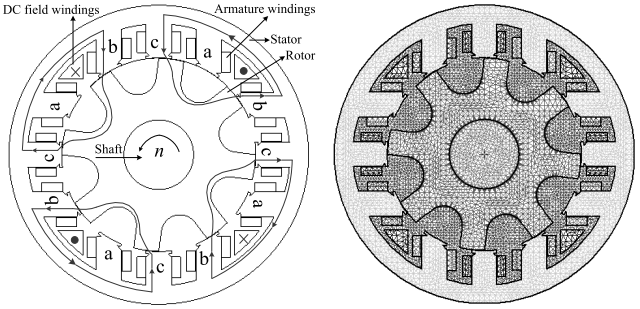

FIGURE 2. Doubly salient electromagnetic generator.

TABLE 1. Critical parameters of DSEG.

Stator outer diameter (mm)	172
Stator inner diameter (mm)	111.4
Stator yoke height (mm)	10.7
Stator tooth height (mm)	19.6
Stator pole arc (°)	15
Rotor outer diameter (mm)	110.9
Rotor inner diameter (mm)	40
Rotor yoke height (mm)	16.2
Rotor tooth height (mm)	19.25
Rotor pole arc(°)	15
Stator and rotor material	1J22
Length of shaft (mm)	60
Rated output voltage (V)	28.5
Rated current (A)	200
Turn-numbers/phase field windings	240
Turn-numbers/phase armature windings	8

are shown in Table 1. The name of each phase winding and rotation direction of generator are defined in Fig. 2. The star and dot signs separately represent for the current flowing into and out of the windings. As can be seen from the structure, every stator tooth is mounted with the concentrated windings, and the stator coils with 90 mechanical degrees interval are connected in series to form a phase winding. There are no copper windings on the rotor, so DSEG is very suitable for high speed running.

When armature windings of DSEG carry the current, phase flux linkage will be constructed and corresponding expressions are given as follows:

$$\boldsymbol{\psi} = [\psi_a, \psi_b, \psi_c, \psi_f]^T \tag{1}$$

where $\boldsymbol{\psi}$ is related to the rotor position and armature current. The flux linkage will change with the variation of the rotor position and armature current, so, electromotive force (EMF) will be produced and its equation is given as follows:

$$\boldsymbol{E} = -\frac{d\boldsymbol{\psi}}{d\theta_r}\frac{d\theta_r}{dt} - \frac{d\boldsymbol{\psi}}{d\boldsymbol{I}}\frac{d\boldsymbol{I}}{dt} = \boldsymbol{e_p} - \boldsymbol{L}\frac{d\boldsymbol{I}}{dt} \tag{2}$$

From above equation, inductive EMF consists of two parts: one is transformer EMF, which is produced by the variation of armature current. The other is rotational EMF and it is induced by the variation of the rotor position.

So, the terminal voltage of respective phase windings can be described by the following equation,

$$\boldsymbol{u} = \boldsymbol{E} - \boldsymbol{RI} \tag{3}$$

where θ_r is rotational angle of the rotor; $\boldsymbol{e_p} = [e_a, e_b, e_c, e_f]^T$ represents for the EMF of each phase windings; $\boldsymbol{I} = [i_a, i_b, i_c, i_f]^T$ are currents of each phase windings; $\boldsymbol{u} = [u_a, u_b, u_c, u_f]^T$ are terminal voltages of every phase windings.

$$\boldsymbol{L} = \begin{bmatrix} L_a & L_{ab} & L_{ac} & L_{af} \\ L_{ba} & L_b & L_{bc} & L_{bf} \\ L_{ca} & L_{cb} & L_c & L_{cf} \\ L_{fa} & L_{fb} & L_{fc} & L_f \end{bmatrix}, \mathrm{R} = \begin{bmatrix} R_a & 0 & 0 & 0 \\ 0 & R_b & 0 & 0 \\ 0 & 0 & R_c & 0 \\ 0 & 0 & 0 & R_f \end{bmatrix}$$

are the inductance matrix and resistance matrix of different windings in DSEG respectively.

B. VOLTAGE REGULATOR

From Fig. 1, voltage regulator provides the dc field current for the field windings of generator, which consists of excitation converter and the controller. Excitation converter contains two MOSFETs and two diodes. The controller can generate PWM signals to drive the switch Q_2 based on some kind of the control law, and Q_1 is on all time. Meanwhile, The controller also detects output voltage of generator and the field current so that it can supply over-voltage and over-current protection.

III. IAF CONTROL STRATEGY IN DSEG

In order to analyze IAF control, we can make the assumption that DSEG works in the following generating stage: the diodes D_1 and D_6 are on state and the current flows by the windings of phase a and b, as shown in Fig.1.

Thus, the sampling value of output voltage, x_1, derivative of x_1, x_2 and the charging current of the capacitor C_o, i_{co}, which can be expressed by following equations,

$$x_1 = \beta u_o \tag{4}$$

$$x_2 = \beta \frac{du_o}{dt} = \frac{\beta}{C_o} i_{co} = \frac{\beta}{C_o}(i_a - \frac{u_o}{R_L}) \tag{5}$$

where u_o is output voltage, β is the ratio, C_o is filter capacitor of generator and R_L is the load resistor.

According to the working stage of the generator in Fig. 1 and neglecting voltage drop of phase resistance, we can get the following equations,

$$u_a = e_a - L_a \frac{di_a}{dt} - L_{ab} \frac{di_b}{dt} \tag{6}$$

$$u_b = e_b - L_b \frac{di_b}{dt} - L_{ba} \frac{di_a}{dt} \tag{7}$$

$$u_o = u_a - u_b, i_a = -i_b \tag{8}$$

where u_a and u_b are the terminal voltages of phase a and b.

Considering $L_{ab} = L_{ba}$, we can acquire the expression of the output voltage from Eqs. (6)-(8),

$$u_o = e_{ab} - (L_a + L_b - 2L_{ab}) \frac{di_a}{dt} \tag{9}$$

So, the current of phase a,

$$i_a = \int \frac{e_{ab} - u_o}{L_a + L_b - 2L_{ab}} dt \tag{10}$$

Substituting Eq. (10) into Eq. (5),

$$x_2 = \frac{\beta}{C_o} \left(\int \frac{e_{ab} - u_o}{L_a + L_b - 2L_{ab}} dt - \frac{u_o}{R_L} \right) \tag{11}$$

So, the derivative of x_1 and x_2 can be expressed

$$\dot{x}_1 = \beta du_o/dt = x_2 \tag{12}$$

$$\dot{x}_2 = \frac{\beta}{C_o} \left(\frac{e_{ab} - u_o}{L_a + L_b - 2L_{ab}} - \frac{1}{C_o R_L} i_{co} \right) = -\frac{x_1}{C_o L} - \frac{x_2}{C_o R_L} + \frac{\beta e_{ab}}{C_o L} \tag{13}$$

where $L = L_a + L_b - 2L_{ab}$.

Remark 1: when the control law u^* make the switch Q_2 turned on, the field current rises and the output voltage of generator gets increased. During this period, the rising rate of the field current depends on the following equation,

$$\frac{di_f}{dt} = \frac{U_f - U_{Q1} - U_{Q2} - i_f R_f}{L_f} \tag{14}$$

The corresponding derivative of x_2 is

$$\dot{x}_2 = \ddot{x}_1 = -\frac{x_1}{C_o L} - \frac{\dot{x}_1}{C_o R_L} + \frac{\beta e_{ab}{}^{\dagger}}{C_o L} \tag{15}$$

where $e_{ab}{}^{\dagger}$ represents for the rising EMF between phase a and phase b when the switch Q_2 is on state.

when the switch Q_2 is turned off under the control law, u^*, the field current decreases and the output voltage of generator gets reduced. At this time, the change rate of the field current can be expressed by the following equation,

$$\frac{di_f}{dt} = -\frac{U_{Q1} + U_{D11} + i_f R_f}{L_f} \tag{16}$$

The corresponding derivative of x_2 is

$$\dot{x}_2 = \ddot{x}_1 = -\frac{x_1}{C_o L} - \frac{\dot{x}_1}{C_o R_L} + \frac{\beta e_{ab}{}^{\ddagger}}{C_o L} \tag{17}$$

where $e_{ab}{}^{\ddagger}$ refers to decreasing EMF between phase a and b as the switch Q_2 is off.

So, the state equation of DSEG can be described as follows,

$$\begin{cases} y = x_1 \\ \ddot{x}_1 = -\frac{x_1}{C_o L} - \frac{\dot{x}_1}{C_o R_L} + \frac{\beta e_{ab}}{C_o L} u^* \\ \quad = f(\boldsymbol{x}) + b_0 u^* \end{cases} \tag{18}$$

where $\boldsymbol{x} = [x_1, x_2]^T$, $b_0 = \beta e_{ab}/(C_o L)$, u^* is the control law of the switch, Q_2, which will affect e_{ab}.

A. DESIGN OF CONTROL LAW

From Eq. (18), we have the optimal control law

$$u^* = \frac{1}{b_0}[\ddot{x}_1 - f(\boldsymbol{x})] \tag{19}$$

The control target is to make x_1 track the given reference voltage signal y_r, the error $e_r = y_r - x_1$. If considering the vector $\boldsymbol{e_r}$=$[e_r, \dot{e}_r]^T$, the second order differential equation of the error is given by

$$\ddot{e}_r = \ddot{y}_r - \ddot{x}_1 \tag{20}$$

Above equation shows the control object is a second order system, and we assume that the second order derivative expression of its error.

$$\ddot{e}_r + k_1\dot{e}_r + k_2 e_r = 0 \tag{21}$$

According to Eq. (21), the characteristic equation of the error is

$$s^2 + k_1 s + k_2 = 0 \tag{22}$$

By choosing appropriate values of k_1 and k_2, which make the roots of Eq. (22) in the left plane of the complex plane, the system is stable ($\lim_{t\to\infty} e_r(t) = 0$). From Eqs. (20) and (21), we have second order derivative of x_1

$$\ddot{x}_1 = \ddot{y}_r + k_1\dot{e}_r + k_2 e_r \tag{23}$$

Substituting Eq. (23) into Eq. (19) yields

$$u^* = \frac{1}{b_0}[\ddot{y}_r + k_1\dot{e}_r + k_2 e_r - f(\boldsymbol{x})] \tag{24}$$

For $f(\boldsymbol{x})$ is unknown, we can consider that design system function estimation $\hat{f}(\boldsymbol{x}|\boldsymbol{\theta})$ to approximate the real system function $f(\boldsymbol{x})$. According to the universal approximation principle of the fuzzy system, we can construct the system function estimation $\hat{f}(\boldsymbol{x}|\boldsymbol{\theta})$ as following:

Step1, define the fuzzy sets of x_1 and x_2, $A_1^{l_1}(l_1 = 1, 2, \cdots, m_1)$ and $A_2^{l_2}(l_2 = 1, 2, \cdots, m_2)$, respectively.

Step2, using $m_1 \times m_2$ fuzzy collection IF-THEN rules to construct the fuzzy system $\hat{f}(\boldsymbol{x}|\boldsymbol{\theta})$, and that is

IF x_1 is $A_1^{l_1}$ and x_2 is $A_1^{l_2}$, THEN $\hat{f}(\boldsymbol{x}|\boldsymbol{\theta})$ is $E^{l_1 l_2}$;

Step3, Assume that the mean value of the fuzzy sets $E^{l_1 l_2}$ is $\bar{y}_f^{l_1 l_2}$, using the product inference, singleton fuzzifier and center-average defuzzifier, the output of the fuzzy system can be acquired

$$\hat{f}(\boldsymbol{x}|\boldsymbol{\theta}) = \frac{\sum_{l_1=1}^{m_1}\sum_{l_2=1}^{m_2}\bar{y}_f^{l_1 l_2}(\prod_{i=1}^{2}\mu_{A_i}^{l_i}(x_i))}{\sum_{l_1=1}^{m_1}\sum_{l_2=1}^{m_2}(\prod_{i=1}^{2}\mu_{A_i}^{l_i}(x_i))} \tag{25}$$

Considering $\bar{y}_f^{l_1 l_2}$ is parameter, which belongs to the sets $\theta \in R^{\prod_{i=1}^{2} m_i}$, meanwhile, constructing the following vector of fuzzy basis functions

$$\boldsymbol{\xi}(\boldsymbol{x}) = [\xi_1(\boldsymbol{x}), \xi_2(\boldsymbol{x}) \cdots, \xi_{m_1\times m_2}(\boldsymbol{x})]^T \tag{26}$$

where $\xi_{(l_1-1)m_2+l_2}(\boldsymbol{x}) = \frac{\prod_{i=1}^{2}\mu_{A_i}^{l_i}(x_i)}{\sum_{l_1=1}^{m_1}\sum_{l_2=1}^{m_2}(\prod_{i=1}^{2}\mu_{A_i}^{l_i}(x_i))}$

Then, Eq.(25) can be expressed by

$$\hat{f}(\boldsymbol{x}|\boldsymbol{\theta}) = \boldsymbol{\theta}^T\boldsymbol{\xi}(\boldsymbol{x}) \tag{27}$$

where $\boldsymbol{\theta} = [\theta_1, \theta_2, \cdots, \theta_{m_1\times m_2}]^T$ and $\boldsymbol{\theta}$ is an adjustable parameter vector.

So, from Eq.(24), we can get

$$u^* = \frac{1}{b_0}[\ddot{y}_r + k_1\dot{e}_r + k_2 e_r - \hat{f}(\boldsymbol{x}|\boldsymbol{\theta})] \tag{28}$$

B. STABILITY ANALYSIS

Substituting Eq.(28) into Eq.(19) and considering Eq.(20), yields

$$\ddot{e}_r = -k_1\dot{e}_r - k_2 e_r + \hat{f}(\boldsymbol{x}|\boldsymbol{\theta}) - f(\boldsymbol{x}) \tag{29}$$

Eq. (29) can be written as below

$$\begin{bmatrix}\dot{e}_r \\ \ddot{e}_r\end{bmatrix} = \begin{bmatrix}0 & 1 \\ -k_2 & -k_1\end{bmatrix}\begin{bmatrix}e_r \\ \dot{e}_r\end{bmatrix} + \begin{bmatrix}0 \\ 1\end{bmatrix}[\hat{f}(\boldsymbol{x}|\boldsymbol{\theta}) - f(\boldsymbol{x})] \tag{30}$$

Define $\boldsymbol{v} = \begin{bmatrix}0 & 1 \\ -k_2 & -k_1\end{bmatrix}$ and $\boldsymbol{c} = [0, 1]^T$, Eq. (30) can be rewritten as vector form

$$\dot{\boldsymbol{e}}_r = \boldsymbol{v}\boldsymbol{e_r} + \boldsymbol{c}[\hat{f}(\boldsymbol{x}|\boldsymbol{\theta}) - f(\boldsymbol{x})] \tag{31}$$

Define optimal parameter

$$\boldsymbol{\theta}^* = \arg\min_{\theta\in\Omega_f}[\sup_{x\in R^n}|\hat{f}(\boldsymbol{x}|\boldsymbol{\theta}) - f(\boldsymbol{x})|] \tag{32}$$

where Ω_f is the sets of $\boldsymbol{\theta}$.

Define the minimum approximation error

$$\omega = \hat{f}(\boldsymbol{x}|\boldsymbol{\theta}^*) - f(\boldsymbol{x}) \tag{33}$$

Substituting Eq.(33) into Eq.(31), we can get

$$\dot{\boldsymbol{e}}_r = \boldsymbol{v}\boldsymbol{e_r} + \boldsymbol{c}[\hat{f}(\boldsymbol{x}|\boldsymbol{\theta}) - \hat{f}(\boldsymbol{x}|\boldsymbol{\theta}^*) + \omega] \tag{34}$$

Considering Eq. (27), rewriting Eq. (34) as

$$\dot{\boldsymbol{e}}_r = \boldsymbol{v}\boldsymbol{e_r} + \boldsymbol{c}[(\boldsymbol{\theta} - \boldsymbol{\theta}^*)^T\boldsymbol{\xi}(\boldsymbol{x}) + \omega] \tag{35}$$

Let us consider the following positive definite function as a Lyapunov function candidate,

$$V = \frac{1}{2}\boldsymbol{e}_r^T\boldsymbol{p}\boldsymbol{e_r} + \frac{1}{2\gamma}(\boldsymbol{\theta} - \boldsymbol{\theta}^*)^T(\boldsymbol{\theta} - \boldsymbol{\theta}^*) \tag{36}$$

where γ is a positive constant called updating coefficient, $\boldsymbol{p}$ is the positive definite matrix satisfying the following condition,

$$\boldsymbol{v}^T\boldsymbol{p} + \boldsymbol{p}\boldsymbol{v} = -\boldsymbol{q} \tag{37}$$

where $\boldsymbol{q}$ is an arbitrary positive definite symmetric matrix, then

$$\dot{V} = -\frac{1}{2}\boldsymbol{e}_r^T\boldsymbol{q}\boldsymbol{e_r} + \boldsymbol{e}_r^T\boldsymbol{p}\boldsymbol{c}\omega + \frac{1}{\gamma}(\boldsymbol{\theta} - \boldsymbol{\theta}^*)^T[\dot{\boldsymbol{\theta}} + \gamma\boldsymbol{e}_r^T\boldsymbol{p}\boldsymbol{c}\boldsymbol{\xi}(\boldsymbol{x})] \tag{38}$$

Then, the adaptive law can be chosen as

$$\dot{\boldsymbol{\theta}} = -\gamma \boldsymbol{e}_r^T \boldsymbol{pc} \boldsymbol{\xi}(\boldsymbol{x}) \tag{39}$$

where γ is the adaptive gain. Substituting Eq. (39) into Eq. (38) yields

$$\dot{V} = -\frac{1}{2}\boldsymbol{e}_r^T \boldsymbol{q} \boldsymbol{e}_r + \boldsymbol{e}_r^T \boldsymbol{pc} \omega \tag{40}$$

As $\boldsymbol{q} > 0$, ω is the minimum approximation error and it can be sufficiently small by designing enough fuzzy rules for fuzzy system to meet $|\boldsymbol{e}_r^T \boldsymbol{pc}\omega| < \frac{1}{2}\boldsymbol{e}_r^T \boldsymbol{q} \boldsymbol{e}_r$ and $\dot{V} < 0$.

The block diagram of IAF control for DSEG is shown in Fig. 3.

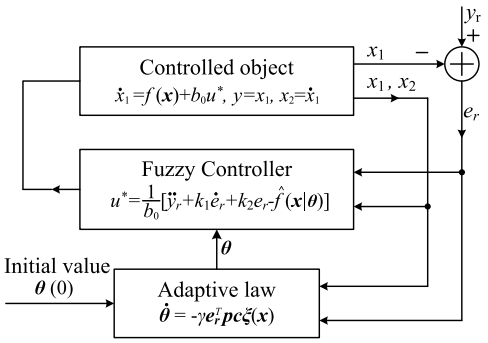

FIGURE 3. Block diagram of IAF control.

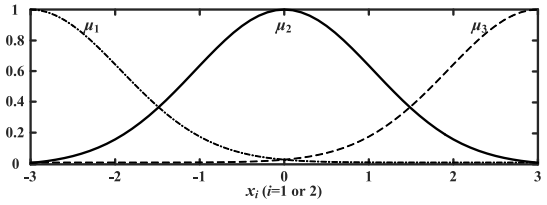

FIGURE 4. Membership functions of x_i ($i = 1, 2$).

C. PARAMETERS SELECTION

In this paper, the membership functions of x_1 and x_2 are defined based on Gaussian-shaped membership functions since they are helpful to acquire better robustness of the system. The corresponding membership functions are given in Eq. (41) - Eq. (43) and the diagram of membership functions are shown in Fig.4.

Moreover, if sufficient numbers of the Gaussian-shaped membership functions are used, control law can be well approximated by $\boldsymbol{\theta}^T \boldsymbol{\xi}(\boldsymbol{x})$ in nonlinear system.

$$\mu_1 = \exp\{-[(x+3)/1.5]^2\} \tag{41}$$
$$\mu_2 = \exp[-(x/1.5)^2] \tag{42}$$
$$\mu_3 = \exp\{-[(x-3)/1.5]^2\} \tag{43}$$

Thus, $m_1 = m_2 = 3$, the variable ranges are $x_1 \in [-3, 3]$ and $x_2 \in [-3, 3]$. The control parameters are $k_1 = 2$, $k_2 = 1$, $\boldsymbol{q} = [10, 0; 0, 10]$, with Eq. (37), We can get $\boldsymbol{p} = [15, 5; 5, 5]$, So, $\boldsymbol{pc} = [5, 5]^T$. Choose $\gamma = 16$, We can get good simulation results.

IV. FIELD-CIRCUIT CO-SIMULATION OF DSEG SYSTEM

Two field-circuit coupling simulation models for DSEG are constructed, as shown in Fig. 5. Fig. 5 (a) exhibits the system model based on fuzzy PID (F-PID) control, while the other model based on IAF control is shown in Fig. 5 (b). The switch Q_1 is always on, So the value of CONST1 is set to 1. The switch Q_2 is driven by PWM signals generated by F-PID or IAF controller. In these models, the value of the supply voltage source U_f is 60V.

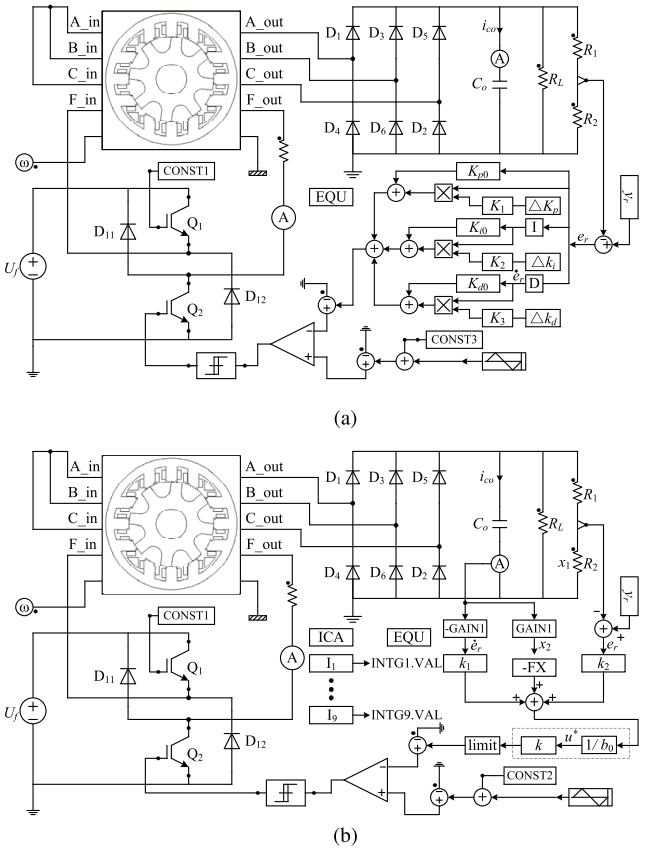

FIGURE 5. System simulation models of DSEG. (a) F-PID control. (b) IAF control.

In Fig. 5 (a), the values of K_{p0}, K_{i0} and K_{d0} are 15, 10, 0.0025, respectively, and $K_1 = 2$, $K_2 = 2$, $K_3 = 0.0005$. The membership functions of e_r, $\dot{e}_r$, ΔK_p, ΔK_i and ΔK_d are shown in Fig.6. The fuzzy rules of ΔK_p, ΔK_i and ΔK_d are shown in Table 2, Table 3 and Table 4. Meanwhile, these fuzzy rules can be described together by 49 conditional statements "If $\cdots$, then $\cdots$", which are written in the model "EQU".

1. If (e_r is NB) and ($\dot{e}_r$ is NB), then (ΔK_p is PB) (ΔK_i is NB)(ΔK_d is PS)
2. If (e_r is NB) and ($\dot{e}_r$ is NM), then (ΔK_p is PB) (ΔK_i is NB)(ΔK_d is PS)
3. If (e_r is NB) and ($\dot{e}_r$ is NS), then (ΔK_p is PM) (ΔK_i is NM)(ΔK_d is ZO)

$\cdots$

49. If (e_r is PB) and ($\dot{e}_r$ is PB), then (ΔK_p is NB) (ΔK_i is PB)(ΔK_d is PB)

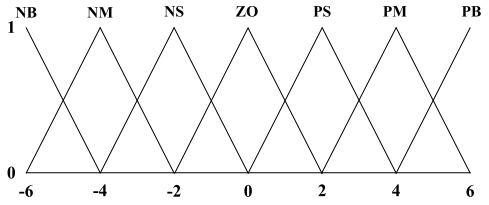

FIGURE 6. Membership functions of e_r, $\dot{e}_r$, ΔK_p, ΔK_i and ΔK_d.

TABLE 2. Fuzzy rules of ΔK_p.

ΔK_p		e_r						
		NB	NM	NS	ZO	PS	PM	PB
$\dot{e}_r$	NB	PB	PB	PM	PM	PS	ZO	ZO
	NM	PB	PB	PM	PS	PS	ZO	NS
	NS	PM	PM	PM	PS	ZO	NS	NS
	ZO	PM	PM	PS	ZO	NS	NM	NM
	PS	PS	PS	ZO	NS	NS	NM	NM
	PM	PS	ZO	NS	NM	NM	NM	NB
	PB	ZO	ZO	NM	NM	NM	NB	NB

TABLE 3. Fuzzy rules of ΔK_i.

ΔK_i		e_r						
		NB	NM	NS	ZO	PS	PM	PB
$\dot{e}_r$	NB	NB	NB	NM	NM	NS	ZO	ZO
	NM	NB	NB	NM	NS	NS	ZO	ZO
	NS	NM	NM	NS	NS	ZO	PS	PS
	ZO	NM	NM	NS	ZO	PS	PM	PM
	PS	NM	NS	ZO	PS	PS	PM	PB
	PM	ZO	ZO	PS	PM	PM	PB	PB
	PB	ZO	ZO	PS	PM	PM	PB	PB

TABLE 4. Fuzzy rules of ΔK_d.

ΔK_d		e_r						
		NB	NM	NS	ZO	PS	PM	PB
$\dot{e}_r$	NB	PS	NS	NB	NB	NB	NM	PS
	NM	PS	NS	NB	NM	NM	NS	ZO
	NS	ZO	NS	NM	NM	NS	NS	ZO
	ZO	ZO	NS	NS	NS	NS	NS	ZO
	PS	ZO	ZO	ZO	ZO	ZO	ZO	ZO
	PM	PB	NS	PS	PS	PS	PS	PB
	PB	PB	PM	PM	PM	PS	PS	PB

So, according to the inputs of fuzzy controller, e_r and $\dot{e}_r$, the values of ΔK_p, ΔK_i and ΔK_d can be determined by above fuzzy rules and centroid defuzzification. Otherwise, The model "I" and "D" in the Fig. 5 (a) represent integral and differential calculus.

The detailed steps to construct IAF control law are illustrated in Fig.7. Firstly, define and initialize variables in "ICA", then programming to acquire membership functions of x_1 and x_2 in "EQU", we can get $\boldsymbol{\xi}(\boldsymbol{x})$ from Eq. (26); Next, we acquire βu_o from voltage of R_2, the error, e_r can be got by y_r minus βu_o; Considering $\gamma = 16$ is a positive constant and $\boldsymbol{pc}$ is the last column of $\boldsymbol{p}$, we can get the adaptive law $\dot{\boldsymbol{\theta}}$ according to Eq. (39). There are 9 elements in $\dot{\boldsymbol{\theta}}$, thus, we need 9 integrators $I_1 \sim I_9$ to acquire the value of $\boldsymbol{\theta}$, then, fuzzy control law u^* can be acquired according to Eq. (28). Finally, PWM driving signal of switch Q_2 can be generated by comparing u^* with the triangular waveform with the constant frequency. In order to prevent the value of u^* beyond the range of the triangular waveform, we need limit the output of the control law by the limiter, and the value of the model, "limit", is ± 1.8. In Fig. 5(b), the value of CONST2 and GAIN1 is 0 and 0.001, respectively, and the amplitude range of the

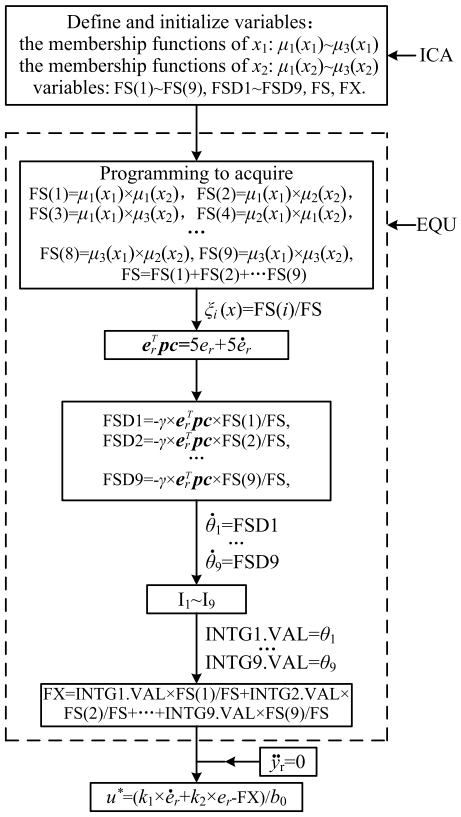

FIGURE 7. Block diagram of IAF control.

triangular waveform is -1.975 to 1.975 while the frequency is 10kHz. From Eq. (18) and considering $e_{ab} = 28.5$V, $\beta = 0.1$, $C_o = 0.04$F and $L = 0.04$H, then b_0 is 1781.25. In order to make the output value of control law fall within the range of the triangular waveform, the value of coefficient k is set to be equal to the value of b_0, and $k = 1781.25$.

A. STEADY STATE ANALYSIS

Load characteristics of the generator at the speed of 4200r/min is shown in Fig. 8. Under the same load increment, the voltage drop under IAF control is apparently smaller than one under F-PID control, which means that IAF control has stronger robustness and influence of load disturbance on generation system is relatively smaller.

Meanwhile, we also show the output waveforms of critical parameters at the load current of 200A under IAF control strategies, as shown in Fig. 9. As can been seen from the output voltage waveforms, we can know that the value of output voltage is about 28.5V, which can track the reference voltage very well. Otherwise, output voltage ripple under IAF control is only 0.7V, which implies that IAF control has excellent steady state response performance.

B. DYNAMIC STATE ANALYSIS

Dynamic performance test is very important for DSEG system. Considering the rated output voltage of DSEG is 28.5V, the simulation waveforms under different controls with the load current increased suddenly form 50A to 200A or reduced

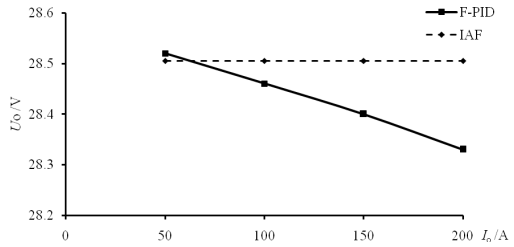

FIGURE 8. Load characteristics at the speed of 4200r/min.

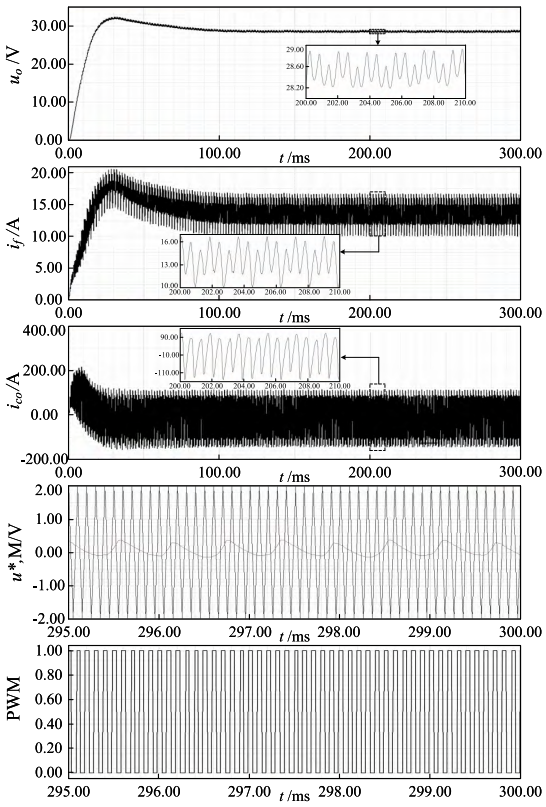

FIGURE 9. Output waveforms of critical parameters under IAF control (n = 4200r/min, I_o = 200A).

suddenly from 200A to 50A at the speed of 4200r/min have been shown in Fig. 10 and Fig. 11. The corresponding data is shown in Table 5. In the Table, ΔU_o represents for the voltage variation with load changed suddenly, t_r is recovery time and m is the number of oscillation;

Seen from the waveforms and data, whenever the load increased or reduced, recovery time and variation of output voltage under IAF control is longer and larger than one under F-PID control. While output voltage ripple under IAF control is smaller than one under F-PID control.

Remark 2: Since the parameters of the controller under IAF control is deduced by Lyapunov stability theory, the steady state performance under IAF control exhibits better. While it takes longer to calculate IAF control law from Eq. (28), the dynamic performance under IAF control is worse than one under F-PID control.

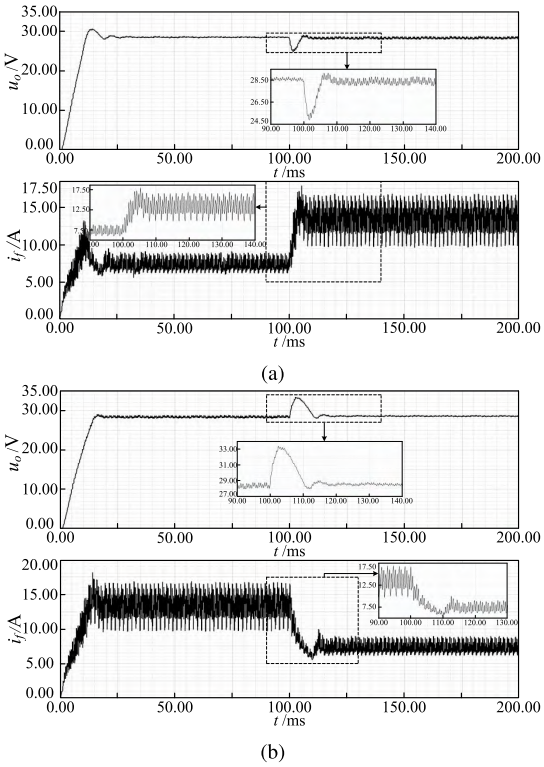

FIGURE 10. Dynamic waveforms under F-PID control. (a) I_o from 50A to 200A. (b) I_o from 200A to 50A.

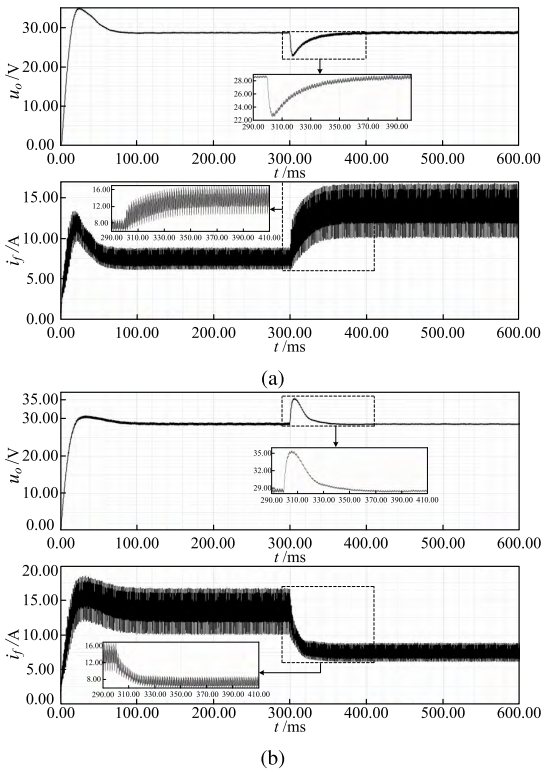

FIGURE 11. Dynamic waveforms under IAF control. (a) I_o from 50A to 200A. (b) I_o from 200A to 50A.

V. CONCLUSIONS

In this paper, a voltage regulation system based on IAF control for DSEG has been proposed, and stability analysis and

TABLE 5. Dynamic characteristics tests (n = 4200r/min.).

Control mode	ΔU_o(V)	I_f(A)	m	t_r(ms)
I_o from 50A to 200A				
F-PID	$\downarrow$ 3.6	7.5 $\rightarrow$ 13.5	1	20
IAF	$\downarrow$ 5.8	7.5 $\rightarrow$ 13.5	1	100
I_o from 200A to 50A				
F-PID	$\uparrow$ 5.3	13.5 $\rightarrow$ 7.5	2	25
IAF	$\uparrow$ 7.2	13.5 $\rightarrow$ 7.5	1	100

the coefficient selection method of IAF controller have been carried out. Then, field-circuit coupling simulation models of DSEG based on F-PID control and IAF control have been constructed. Moreover, we can draw following conclusions by comparing the results under F-PID control with ones under IAF control.

(a) Output voltage drop under IAF control is smaller than one under F-PID control with the same load increment in steady state, which proves that IAF control has better robustness; Moreover, the generation system under IAF control also acquires good steady state characteristics;

(b) Output voltage ripple of generator under IAF control is smaller than one under F-PID control;

(c) During dynamical tests, recovery time and voltage variation of output voltage under IAF control are longer and larger than ones under F-PID control.

ACKNOWLEDGMENT

The authors would like to thank to all those involved in the studying program and in the preparation of this paper.

REFERENCES

[1] Y. Liao and T. A. Lipo, "Sizing and optimal design of doubly salient permanent magnet motors," in *Proc. 6th Int. Conf. Electr. Mach. Drives*, Oxford, U.K., Sep. 1993, pp. 452–456.
[2] M. Cheng, Q. Sun, and E. Zhou, "New self-tuning fuzzy PI control of a novel doubly salient permanent-magnet motor drive," *IEEE Trans. Ind. Electron.*, vol. 53, no. 3, pp. 814–821, Jun. 2006.
[3] Y. Fan, K. T. Chau, and M. Cheng, "A new three-phase doubly salient permanent magnet machine for wind power generation," *IEEE Trans. Ind. Appl.*, vol. 42, no. 1, pp. 53–60, Jan. 2006.
[4] X. L. Meng, L. Wang, and Y. G. Yan, "Novel field-winding doubly salient brushless DC generator," (In Chinese) *Trans. China Electrotech. Soc.*, vol. 20, no. 11, pp. 10–15, Nov. 2005.
[5] Y. Fan, K. T. Chau, and S. Niu, "Development of a new brushless doubly fed doubly salient machine for wind power generation," *IEEE Trans. Magn.*, vol. 42, no. 10, pp. 3455–3457, Oct. 2006.
[6] Y. Li and T. A. Lipo, "A doubly salient permanent magnet motor capable of field weakening," in *Proc. 26th Annu. IEEE Power Electron. Specialists Conf.*, Atlanta, GA, USA, Jun. 1995, pp. 565–571.
[7] Z. Chen, B. Wang, Z. Chen, and Y. Yan, "Comparison of flux regulation ability of the hybrid excitation doubly salient machines," *IEEE Trans. Ind. Electron.*, vol. 61, no. 7, pp. 3155–3166, Jul. 2014.
[8] Q. Le, Z. R. Zhang, and Y. Y. Tao, "Comparative study of three kinds of doubly salient BLDC generators," in *Proc. Int. Conf. Electr. Mach. Syst.*, Beijing, China, Aug. 2011, pp. 1–5.
[9] W. L. Dai, Y. B. Li, H. Z. Wang, and Y. G. Yan, "Dual output voltage regulator of doubly salient electro-magnetic generator," (In Chinese) *Proc. CSEE*, vol. 28, no. 23, pp. 105–111, Aug. 2008.
[10] W. L. Dai, J. Ding, and H. Tian, "Analysis and simulation for voltage regulation system of doubly salient electro-magnetic generator based on sliding mode control," in *Proc. 33rd Chin. Control Conf.*, Nanjing, China, Jul. 2014, pp. 8064–8069.
[11] S. Tong, P. Shi, and H. Al-Madfai, "Robust fuzzy decentralized control for nonlinear large-scale systems with parametric uncertainties," *J. Intell. Fuzzy Syst.*, vol. 19, no. 2, pp. 85–101, 2008.
[12] M. H. Khooban and M. R. Soltanpour, "Swarm optimization tuned fuzzy sliding mode control design for a class of nonlinear systems in presence of uncertainties," *J. Intell. Fuzzy Syst.*, vol. 24, no. 2, pp. 383–394, 2013.
[13] A. F. Attia, Y. A. Al-Turki, and H. F. Soliman, "Genetic algorithm-based fuzzy controller for improving the dynamic performance of self-excited induction generator," *Arabian J. Sci. Eng.*, vol. 37, no. 3, pp. 665–682, Apr. 2012.
[14] L. X. Wang, "Stable adaptive fuzzy control of nonlinear systems," *IEEE Trans. Fuzzy Syst.*, vol. 1, no. 2, pp. 146–155, May 1993.
[15] C. J. Zhou, D. C. Quach, N. X. Xiong, S. Huang, Q. Zhang, and Q. Yin, "An improved direct adaptive fuzzy controller of an uncertain PMSM for Web-based E-service systems," *IEEE Trans. Fuzzy Syst.*, vol. 23, no. 1, pp. 58–71, Feb. 2015.
[16] S. Labiod and T. M. Guerra, "Direct adaptive fuzzy control for a class of MIMO nonlinear systems," *Int. J. Syst. Sci.*, vol. 38, no. 8, pp. 665–675, Aug. 2007.
[17] P. A. Phan and T. J. Gale, "Direct adaptive fuzzy control with a self-structuring algorithm," *Fuzzy Sets Syst.*, vol. 159, no. 8, pp. 871–899, 2008.
[18] M. Wang, B. Chen, and S. L. Dai, "Direct adaptive fuzzy tracking control for a class of perturbed strict-feedback nonlinear systems," *Fuzzy Sets Syst.*, vol. 158, no. 24, pp. 2655–2670, 2007.

WEILI DAI (M'09) was born in Jiangsu, China, in 1979. He received the B.S. degree in electrical engineering and automation from the Institute of Technology, Yangzhou University, Yangzhou, China, in 2001, and the M.S. and Ph.D. degrees in power electronics and motor drive from the Nanjing University of Aeronautics and Astronautics, Nanjing, China, in 2004 and 2008, respectively.

He is currently an Associate Professor with the College of Internet of Things Engineering, Hohai University, Changzhou, China. He has authored and co-authored 20 journal publications and 12 conference papers. He holds ten patents in the area of electrical machine control. His current research interests include the design and advanced control of new electrical machines, wireless power transfer technology, and electromagnetic analysis of electrical equipment.

YANGHUA YU was born in Jiangsu, China, in 1991. He received the B.S. degree in automation from the College of Internet of Things Engineering, Hohai University, Nanjing, China, in 2015, where he is currently pursuing the master's degree in detection technology and automatic equipment. His current research interests include advanced control theory in doubly salient generator and motor drive.

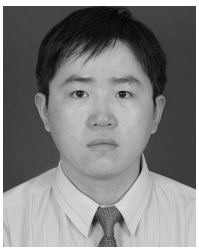

MINGANG HUA (M'14) was born in Jiangsu, China, in 1980. He received the Ph.D. degree from the South China University of Technology, Guangzhou, China, in 2009. He is currently an Associate Professor with the College of Internet of Things Engineering, Hohai University, Changzhou, China. His current research interests include nonlinear systems, stochastic systems and Markovian jumping systems.

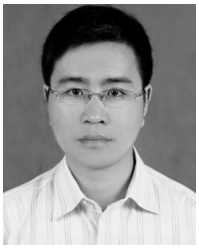

CHANGCHUN CAI was born in Zhejiang, China, in 1981. He received the B.S., M.S., and Ph.D. degrees from Hohai University, Nanjing, China, in 2003, 2007, and 2012, respectively. He is an Assistant Professor with the Central of Power Transmission and Distribution, Hohai University, and a Visiting Scholar with the University of Tennessee. His current research interests include microgrid operation and control, power system modeling, and smart grid.